Determination of physical properties and thermal conductivity of graphite foam with image analysis

Amir Mohammadimehr *[a], İsmail Solmus [a], Baris Ozyer [b], D. Andrew S. Rees[c]
[a] Department of Mechanical Engineering, Ataturk University, Erzurum, Turkey
[b] Department of Computer Engineering, Ataturk University, Erzurum, Turkey
[c] Department of Mechanical Engineering, University of Bath, Bath BA2 7AY, UK
E-mail: amir.mohammadimehr141@ogr.atauni.edu.tr*, solmus@atauni.edu.tr, baris.ozyer@atauni.edu.tr, D.A.S.Rees@bath.ac.uk

REFERENCE NO

Ref # 1-31

Keywords:

Graphite foam
Image Analysis
Porosity
3D reconstruction
Specific surface area
Effective thermal conductivity

Abstract

Since pore network structures of porous materials have irregular shapes and may vary in size, the accurate characterization and virtual 3D reconstruction of these materials is of great importance for a deeper understanding of the structure and subsequent calculations. In this study, the Scanning Electron Microscope (SEM) and X-ray micro Computed Tomography (μCT) images of a graphite foam sample are used for Image Analysis Method (IAM) and virtual 3D reconstruction as non-destructive scientific tools with high accuracy. The morphological characterization and determination of effective pore diameter, porosity, specific surface area (SSA) and effective thermal conductivity (ETC) of POCO graphite foam are investigated. By examining the results obtained from the method of image analysis, it is found that there is a good agreement among the IAM results.

1. Introduction

Porous materials are cellular materials which are made of interconnected solid struts that enclose cells and pore regions [1]. These materials have many prominent properties such as a lightweight structure, a higher thermal expansion coefficient, a high conductivity, a homogenous microstructure and isotropy which make them suitable for various applications. For example, these materials are widely used in aerospace and biomedical applications, fuel cells, energy storage, heaters, heat exchangers, reactors and thermal management systems [2,3].

The characterization and understanding of the structural properties of graphite foam play a key role in determining the effectiveness of this kind of porous material depending on the working conditions for specific applications [4,5]. In general, geometry, morphology and porosity are defined as structural properties of porous materials. Geometry in porous materials is described as a combination of the effective pore diameter, cell size and the distances between the pores [6,7]. There is also a standard categorization that divides the pores into three main groups: micropores (<2 nm), mesopores (2-50 nm) and macro pores (>50 nm) [8]. The morphology is related to the shape of the pores, interactions and orientations. Porosity is the most important feature when defining the physical properties of porous materials. It is described as the fraction of the volume of voids over the total volume and is a number ranging from 0 to 1. The knowledge of such physical properties is important since they have a strong impact on the thermal properties of porous materials, for example, the effective thermal conductivity.

There are several laboratory methods that are used to characterize the pore morphology of porous materials such as pore size and pore size distribution (PSD) [9,10], porosity [11] and SSA [12]. These laboratory methods include Brunauer-Emmett-Teller (BET) [13], mercury intrusion porosimetry [14] and the microscopic method [15]. However, each of these methods has its own limitations: (i) the sample can be damaged during the experiment; (ii) in the case of closed-cell foams, the common laboratory methods cannot be applied to obtain the morphological parameters; (iii) these methods are not able to provide a virtual three dimensional model in order to find out more about the geometrical and physical properties of the porous structure. They also do not give direct information about the pore shape or size for each pore.

Because of the limitations of the experimental methods given above, Image Analysis Methods (IAM) on the other hand, have been studied extensively to analyze the structural and thermal properties of porous materials during the last decades. The researchers previously used IAM on Scanning Electron Microscopy (SEM) images of porous filtration membranes [6,10], aluminum foam [16], air-entrained concrete [17], porous pavements [18] and porous silicon layers [7]. They successfully obtained some morphological parameters for these materials. The accuracy of the process is based on the distribution of the pores on the surface and on the pore size. For instance, a membrane is a kind of porous material, composed of nano pores whose corresponding SEM images include a large number of pores (in a square micron) compared to the samples with macro pores, so this factor makes the SEM images suitable for IAM. However, in this study, graphite foam is composed of macro pores so the analysis of its structural properties using SEM images is not sufficiently accurate to obtain its physical properties and then the effective thermal conductivity of graphite foam materials. The use of IAM on X-ray micro computed tomography (μCT) images is another way of measuring the physical properties of materials. This method uses X-rays to create cross-sections of a physical object that may be used to recreate a virtual 3D model [19-23] without destroying the sample. Micro-CT has many applications both in medical imaging and in industrial computed tomography [24]. It can provide us with the ability to visualize the internal structure of materials in a fully 3D environment.

In this study, the physical properties and effective thermal conductivity (ETC) of graphite foam based on the structural properties of the samples are analyzed. Graphite foams are characterized by having interconnected open cell macro pores. Due to this structure, it has a significant ETC. This paper forms a pioneering study whereby the structural and thermal properties of graphite foam and the relationship between them are investigated by using the IAM and virtual 3D reconstruction method with the application of X-ray micro computed tomography (μCT) and a SEM imaging system. The main contributions of the paper are as follows: (i) The morphological and physical properties of graphite foam such as pore size, PSD, porosity, SSA are characterized for the first time. We then calculated the ETC [25-29] with IAM by using SEM and X-ray μCT Images on the open-source software, ImageJ [30], (ii) We also successfully obtained the morphological parameters and SSA by using the virtual 3D reconstruction method on Imorph [31], (iii) By examining the results and comparing them we found that there is a direct relationship between the physical and thermal conductivity of graphite foam, (iv) Furthermore, we successfully demonstrated the homogeneity of the graphite foam material, (v) We verified experimentally that the data obtained from 2D IAM are in good agreement with the data acquired by a virtual 3D model, which also confirms the correctness and validity of IAM on 2D images. Finally, the results obtained are discussed and compared with information provided by the manufacturer. The validity and accuracy of the present image analysis and virtual 3D reconstruction methods are verified experimentally.

2. Methodology

In this section, we introduce our proposed method to calculate the physical properties and effective thermal conductivity of a graphite foam sample with image analysis techniques. The results obtained are then compared with the manufacturer's data. The flow chart of our proposed methods is shown in Fig. 1. The characterization of the physical properties and thermal conductivity of graphite foams is essential for consumers as they need this information for the accurate prediction of the behavior and performance of such foams that will then inform the choice of the appropriate type of graphite foam for the desired industrial application.

First, graphite foam samples are prepared in the proper dimensions and thin layers for image acquisition and the laboratory process. Second, SEM and μCT images of graphite foam samples are obtained. Third, as a preprocessing step, the physical properties of graphite foam with IAM, for both SEM and μCT 2D images are calculated. Fourth, by using the fundamental heat transfer equations and the data obtained at the previous stage, the ETC of graphite foam is computed. In addition to using 2D image analysis for the calculation of its physical properties, we have used a 3D reconstructed virtual model of graphite foam and obtained physical properties such as porosity and SSA directly.

In addition to using IAM, the BET laboratory method is applied to the sample. Even though there are some limitations using laboratory methods for this kind of material, the geometrical and physical parameters of the sample such as its average pore diameter, its BET surface area, and its cumulative pore volume are obtained.

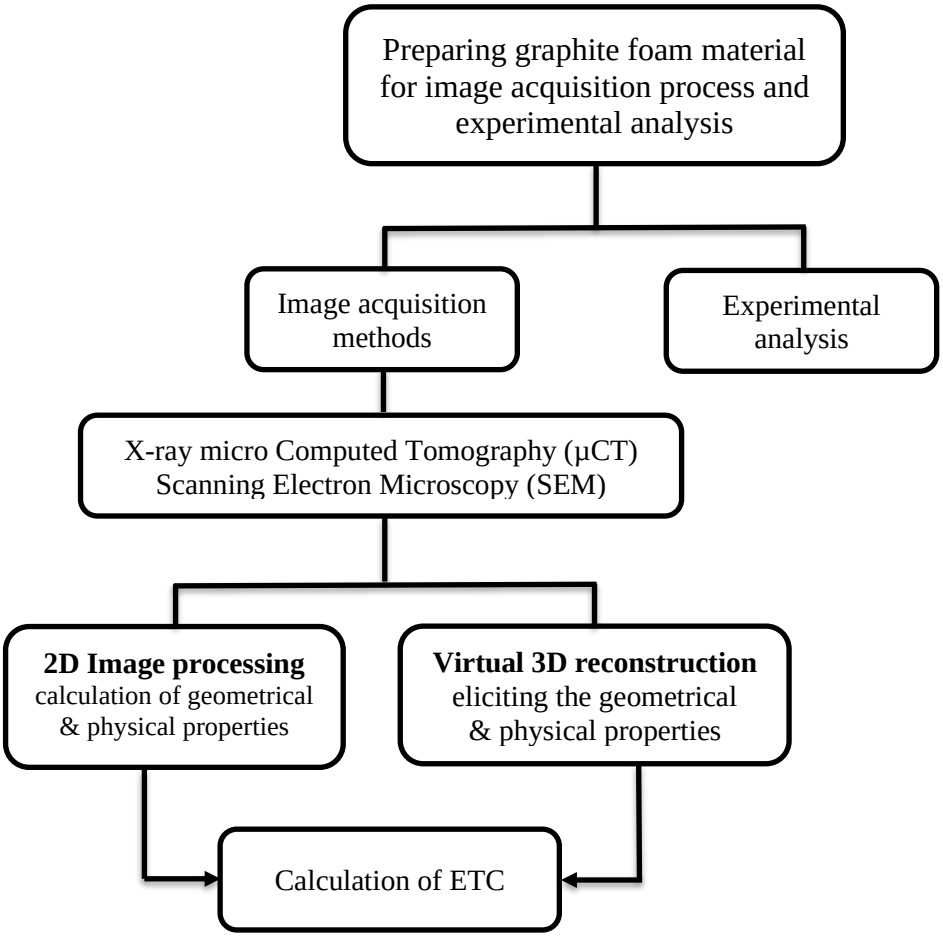

Fig. 1 Flow chart of image analysis of graphite foam

2.1. Material and Sample Preparation for Image Acquisition

2.1.1. Material

In this study, a piece of graphite foam sample, manufactured by POCO, USA, with various pore sizes, irregular shapes, and total porosity of 75% is used in order to analyze its physical properties and the calculation of its effective thermal conductivity (ETC), see Fig. 2. As for its crystalline structure, we observe that POCO graphite has a typical hexagonal structure. The layer spacing may vary though, as it is a function of raw material and process conditions which vary from manufacturer to manufacturer but then POCO graphites are also highly isotropic with respect to their structure and properties. Being highly isotropic means that its properties are identical independently of the direction of measurement. We mention this because many conventional graphites are formed as anisotropic. The high degree of isotropy makes POCO graphites useful in many applications where an anisotropic material would either fail or be unsuitable. It also allows for maximum utilization of such material, as machining orientation is of no importance.

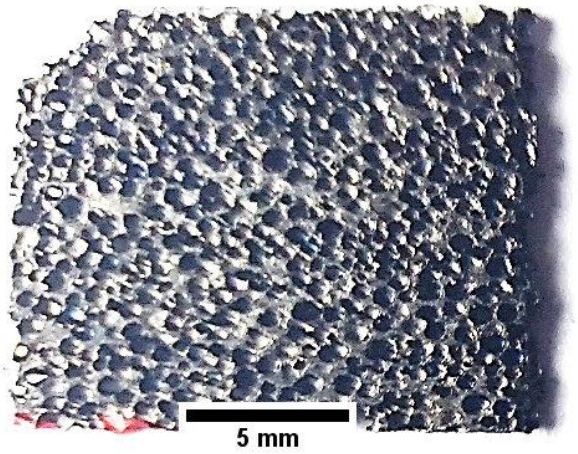

Fig. 2 Original image of POCO graphite foam

2.1.2. Sample preparation

The initial dimensions of the samples prior to cutting were about 22×16×13 mm. These were then cut down by means of a wire electrode cutting machine to a size of 16×13×1 mm for use in imaging procedures and laboratory analyzes. It should be emphasized that we should cut the slices as thinly as possible without any geometrical and structural deformation as this preparation will have a great influence on the quality of the samples and on subsequent results. Due to the nature of the sample and its fragility, other cutting techniques or polishing methods are not recommended.

2.2. Image Acquisition

Two types of images of the graphite foam layers are provided for calculating their geometrical and physical properties in IAM. The first type of image is taken by the Scanning Electron Microscope (SEM), ZEISS Sigma 300 in the east *Anatolia high technology application and research center* at Ataturk University also known as DAYTAM. A typical SEM image of graphite foam as a grayscale 8-bit image with a size of 1024×768 pixels is shown in Fig. 3. The image acquisition conditions include the observation range, the working distance, the amount of magnification and the accelerating voltage, all displayed in the data zone. For example, referring to Fig. 3, we see that the working distance (WD) between the sample surface and the lower pole piece is 18.8 mm. Similarly, the accelerating voltage (EHT) and magnification parameters (MAG) are set to 15.00 kV and 24 X, respectively.

As shown, it is not easy to identify the structural details of pores on two-dimensional SEM images as opposed to the virtual 3D model of graphite foam. The reason for this is that the incident electron beam reflects from the specimen surface and does not pass through the specimen. On the other hand, in X-ray micro computed tomography, radiation passes through the specimen and consequently it is well able to provide more structural details arising from within the sample.

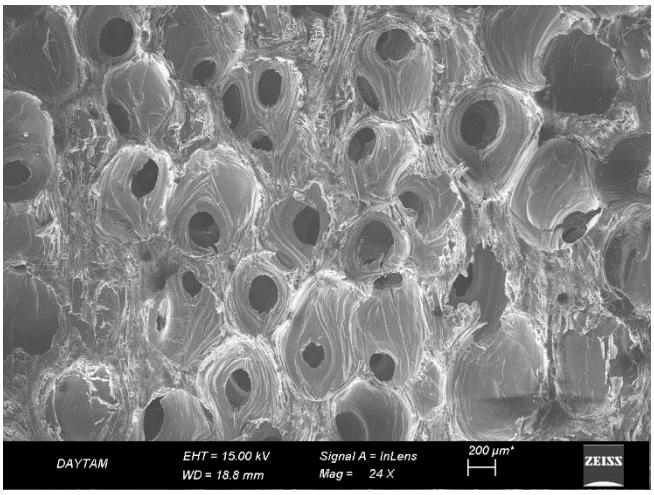

Fig. 3 A SEM image of graphite foam (at the scale of 50% of original image)

The second type of images having a size of 2000 × 2000 pixels (1287 slice images) are taken by an X-ray micro computed tomography (µCT) Skyscan 1172 in the BIOMATEN (Center of Excellence in Biomaterials and Tissue Engineering), at Middle East Technical University (METU), Biotechnology Research Unit. Here 2D slice images and cross-sectional images of the sample are shown in Fig. 4a and Fig. 4b, respectively. The acquisition conditions such as source voltage (kV), source current (µA) and the image pixel size (µm) were selected as 59, 167 and 10.035, respectively.

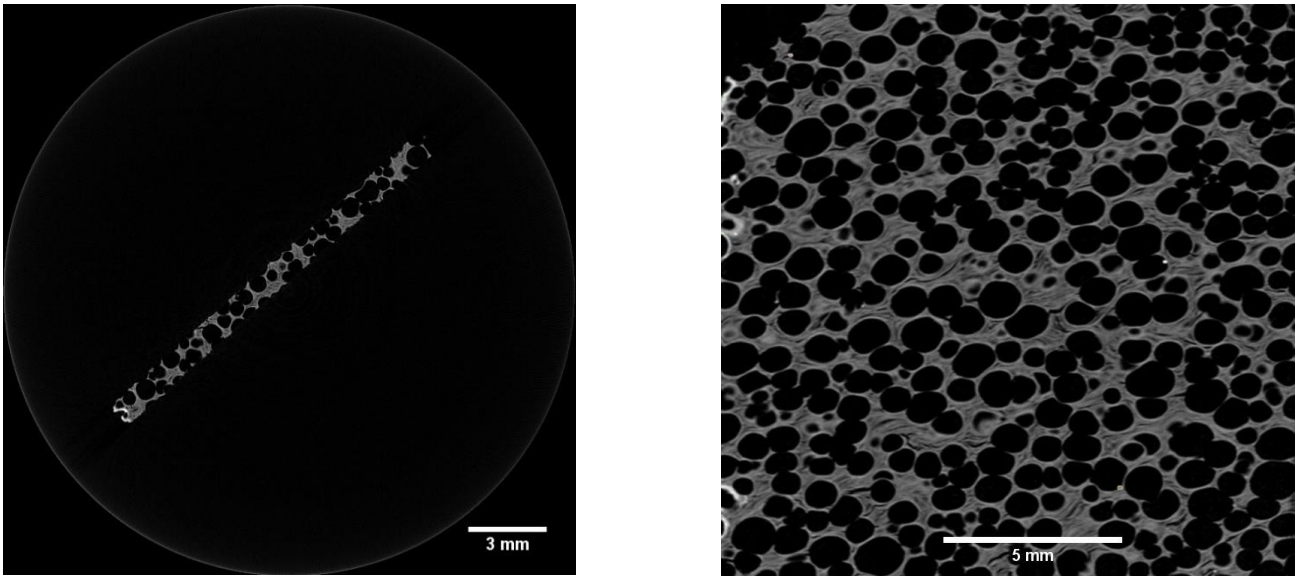

(a) **(b)**

Fig. 4 µCT images of graphite foam.
(a) The 2D slice images (b) The cross-sectional image

2.3. Image Analysis

In this section we first describe the preprocessing steps that are used to obtain binary images from 2D SEM and µCT gray-scale original images in order to calculate their geometrical and physical properties.

2.3.1 Preprocessing

Step 1: **Set Scale**

In order to analyze the procedure, the input image should be scaled, and the proper measurement unit should be determined with regards to the pore size and scale bar both of which are usually located on the data zone of the images. For this we used ImageJ, a Java-based image processing program as follows: By considering the dimensions of the sample on the original images using the scale bar and then applying the proper scale on these images, we were able to obtain results based on the specified units at the end of the analysis and calculations.

Step 2: **Crop the original image**

Cropping the image is a process that separates the Region of Interest (ROI) from the entire original image. In this step, the dimensions of the input images were fixed at 1274×1120 pixels as the ROI. For example, a cross-sectional image of the sample is shown in Fig. 5a.

Step 3: **Image enhancement**

Image enhancement techniques bring out details in an image that is obscured, or they may highlight certain features of interest therein. Image enhancement operations typically return a modified version of the original image and are frequently used as a preprocessing step in order to improve the results of image analysis techniques. We first made a manual adjustment to the pixel intensity values of the cropped image so as to enhance contrast. Then a median filter was applied to the image by removing noise, as shown in Fig. 5b.

Step 4: **Global thresholding based on the Otsu method**

The Otsu method applied to images is used to convert them from gray scale to binary images. The Otsu method automatically performs clustering-based image thresholding or the reduction of a gray level to a binary image. Typically, the two colors used for a binary image are black and white. The color used for the object(s) in the image is the foreground color while the rest of the image is the background color. In this method, the intraclass variance of pixel intensities of the black and white pixels is minimized and the between-class variance is maximized, as shown in Fig. 5c.

Step 5: **Image Filtering**

After thresholding, we obtained binary images in which the black color represents the solid region while the white color represents the pore regions. However, as shown in Fig. 5c, there are some small objects and features next to the pore region mainly created by the incident electron beam in SEM or using X-rays in a CT imaging system. It is known as noise and this remains also after image thresholding (step 4). Median filtering is applied on the images to remove these noises, as shown in Fig. 5d. This method reduces the noise in the active image by replacing each pixel value with the median of the neighboring pixel values.

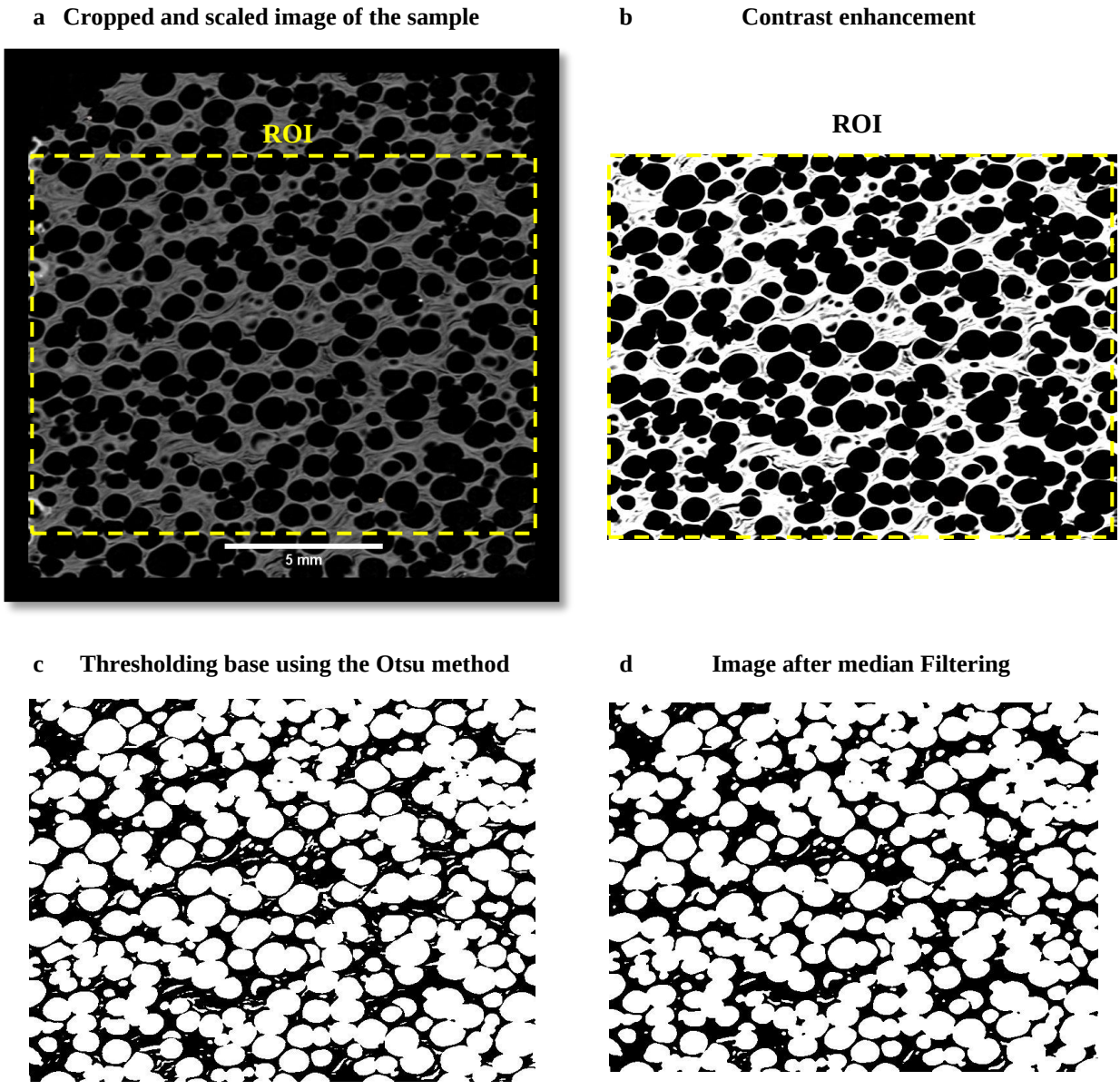

Fig. 5 Preprocessing steps for the µCT Images of graphite foam

In the last step of image preprocessing, the porosity is determined directly from the images based on the fraction of the area of the pore regions to the entire region of the binary image.

2.3.2 Implementing distance map and find maxima functions

In this step, the effective pore diameter of graphite foam defined as the diameter of the largest possible virtual circle enclosed by pixels with zero values in the binary image is calculated. For this, we have used the *distance map* and *find maxima* functions on the given images respectively to find the local maximum value (M), necessarily located at the center of each pore blob.

First, we use the *distance map function* which measures the separation of points on the image and calculates the distance between each pixel that is set to zero (off) and the nearest nonzero pixel for binary images. Secondly, as shown in Fig. 6., which represents a schematic of the process, we found different values for M as a local maximum of the pixel values that are located at the center of each pore blob by using the *Find Maxima* function for a binary image. The radius of the effective pore diameter for each pore blob is then defined as the distance between the center of the virtual circle (M, the pixel with maximum value in the pore region) and its nearest edge point (nonzero pixel) in the pore region. The reason for choosing the nearest non-zero edge point is that, according to Fig. 6d, if we chose the furthest point, the virtual circle could include pixel values starting at 0 and greater in the distance transformed image and cover pore and non-pore regions. In other words, if there were narrow channels between the pores, the diameter of the virtual circle could be bigger and cover other nearby pore regions which could then be considered as one pore region. This would then affect the results of our calculations adversely.

The details of these final steps, the binarized image, the assigned values for each pixel, the distance-transformed image and the finding of the local maximum value (M) in each pore region are illustrated in Fig. 6.

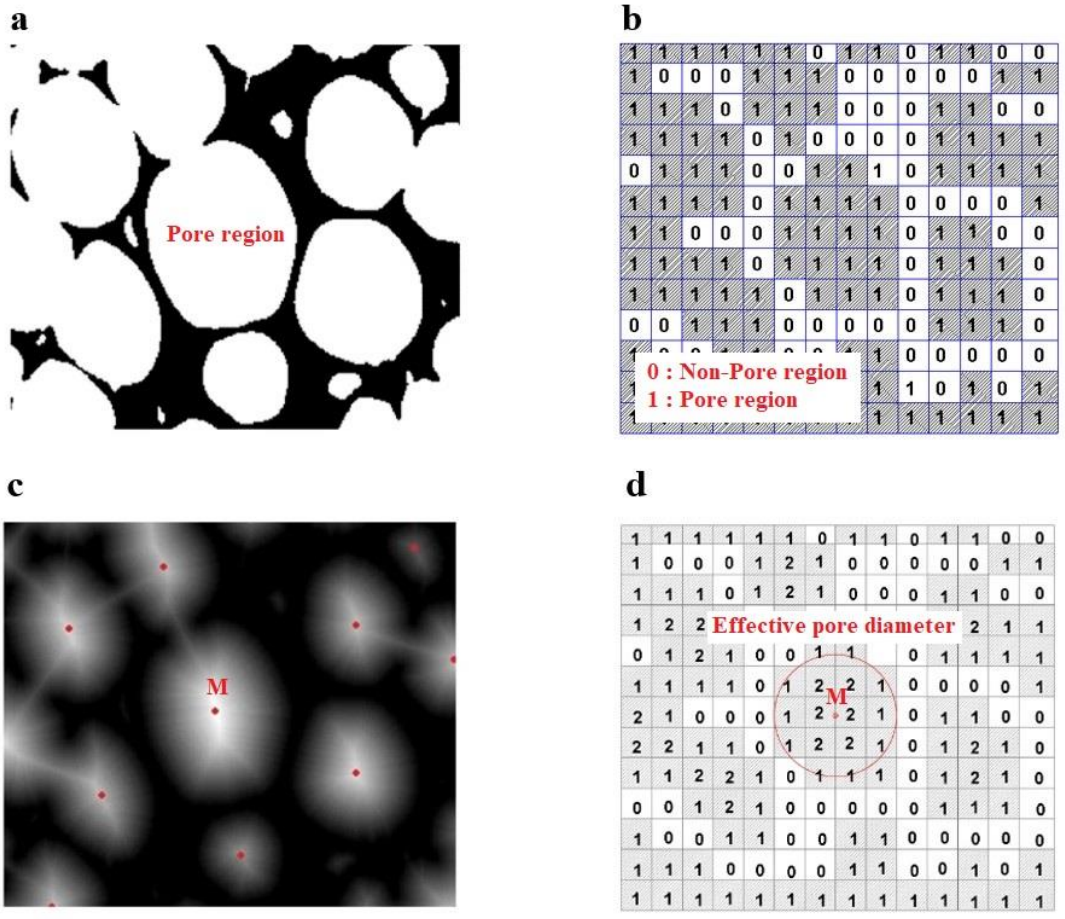

Fig. 6 Schematic of the binarized image (a) and assigned value for each pixels (b), Distance transformed image (c) and finding the local maximum value for each pore region (d)

The mathematical representation of local maximum value (**M**) for each pore region can be expressed as follows [6]:

$$M(x,y) = \max\{DT(x,y)\}, \;\; P(x,y) \in A \tag{1}$$

Where *A* is the pore region, *P* is the pixels in the pore regions, *DT(x,y)* is the minimum distance from the pixel *P*(*x*,*y*) to the non-pore region. The area (A_p) of a pore blob is computed as follows:

$$A_p = m, \tag{2}$$

where m is the number of pixels contained in a pore blob. The distance-transformed image and Find-Maxima function (for finding the center of each pore blob) with its magnified image are presented in Fig.7a, 7b and 7c, respectively.

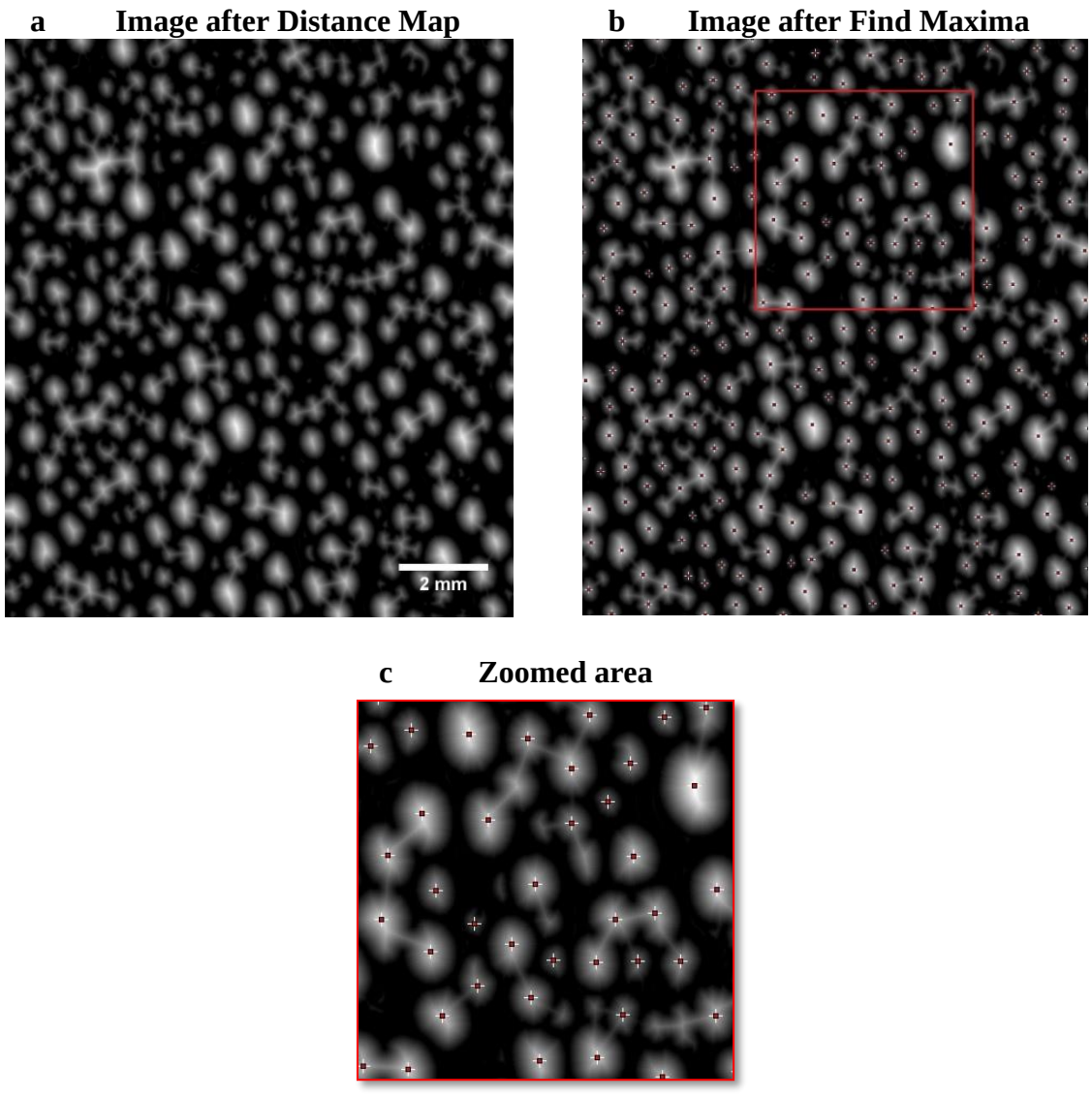

Fig. 7 The distance transformed image (a) and finding the local maximum value in the pore regions (b) Enlarged image (c)

Fig. 7c., clearly shows that almost all the existing pore centers were selected in a precise manner on the images. With a careful examination of these images, we found that although there is noise in some parts of the images, beside the pore regions or very narrow channels between the pores, adjacent pores were not considered as a single pore in the selection procedure. Channels or other small objects were ignored by the Find Maxima function in this case. This function precisely detected the center points of each single pore blob and identified them with a point mark in red (as defined).

In order to obtain the numerical values of (M) for each pore blob on the whole distance transformed image we have followed *Process* > *Find Maxima* on the ImageJ. In the field of noise tolerance, we've adjusted the approximate noise size for detecting the process of every single pore. The amount of noise tolerance was selected on the basis of the consideration of the primary knowledge of randomly measured image pore sizes. This can be done by changing the value of the noise tolerance until all the intended pores were selected independently. In other words, we should know at what size range pores are generally placed so as to prevent selecting many connective pores together, then considered as one pore, or by selecting the unnecessary areas such as the noises that we're unable to remove completely by conventional filtering functions. At the end of this step, we obtained all the maximum values of each pore blob including the number of pores on the image (about 260 pores) along with their coordinates and other such information. It should be notice that the unit of the computed local maximum values (M) for each pore region is in pixels (based on the pixel intensity). So, the local maximum values which gives the distance between the center of a pore to the nearest non-pore region should be converted to microns for further calculations. Since we know the dimensions of the images and the size of each single pixel, we're able to make this conversion. In Table 1 we illustrate a small portion of the exported data sheet.

	Label	Mean	Mode	Min	Max	X	Y
1	ROI.jpg	45	45	45	45	814	234
2	ROI.jpg	44	44	44	44	509	852
3	ROI.jpg	43	43	43	43	9	755
4	ROI.jpg	42	42	42	42	965	1139
5	ROI.jpg	42	42	42	42	1007	878
6	ROI.jpg	41	41	41	41	493	1221
7	ROI.jpg	41	41	41	41	16	1039
8	ROI.jpg	41	41	41	41	292	354
9	ROI.jpg	40	40	40	40	615	1045
10	ROI.jpg	40	40	40	40	202	285
11	ROI.jpg	40	40	40	40	532	170
12	ROI.jpg	39	40	40	40	423	400
13	ROI.jpg	38	39	39	39	704	659
14	ROI.jpg	38	38	38	38	1111	578
15	ROI.jpg	38	38	38	38	373	468
16	ROI.jpg	38	38	38	38	1110	468
17	ROI.jpg	38	38	38	38	892	419
18	ROI.jpg	38	38	38	38	474	269
19	ROI.jpg	37	37	37	37	581	1252
20	ROI.jpg	37	37	37	37	424	808

Table.1 The various values of M obtained

In addition, we're able to identify the pixels' value (listed in Table 1) along with their coordinates manually, as shown in Fig. 8.

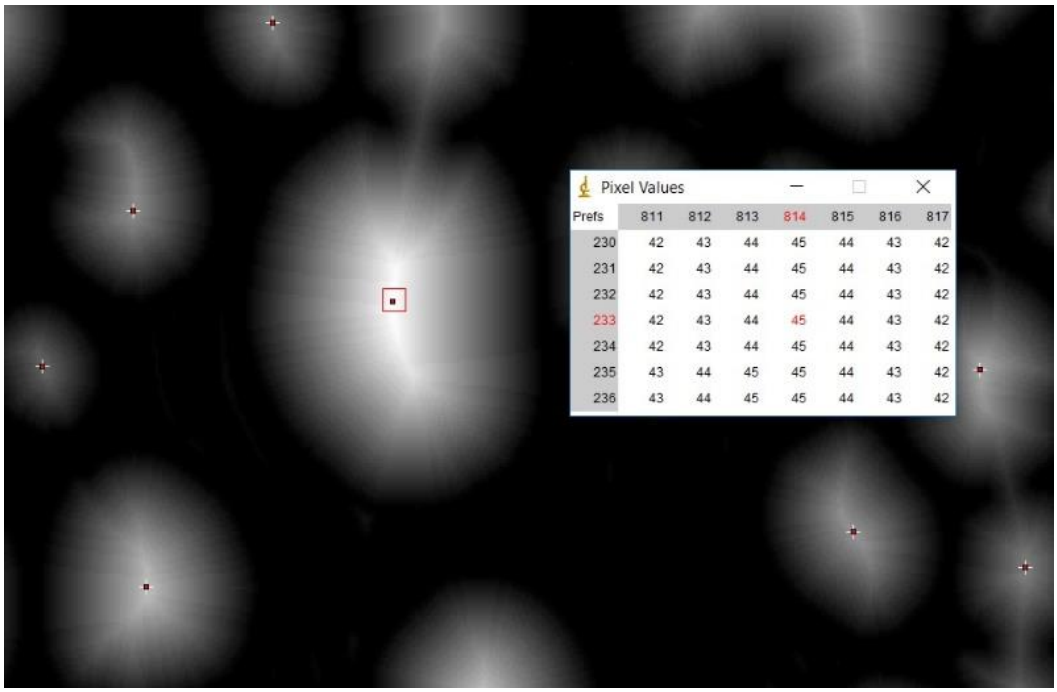

Fig. 8 The details of using a pixel inspector on the images

2.4. Calculation of Physical Properties and ETC

From the preprocessed images and the comprehensive geometrical data that were obtained in section 2.3., the number of parameters and their distributions can be calculated using the equations and analytical methods proposed in [5]. These parameters include: the effective pore diameter (in microns), the PSD, the porosity (%), the SSA, ETC., and so on. A set of parameters is calculated for each pore blob and the radius of each pore blob is calculated as follows (on account of the pixel width):

$$\mathrm{R}(\mu) = M - 0.5 \tag{3}$$

where R is the calculated radius for each pore blob defined by using $\boldsymbol{M}$ (the local maximum value of each pore) defined earlier at the center of each pore blob. Since the local maximum value in the pore region gives the distance between the center of the pore region and its closest nonzero pixels (the radius of the pore blob), therefore the effective pore diameter for this pore blob is given by:

$$D_{eff}\ (\mu) = 2, R \tag{4}$$

The effective pore diameter is one of the most useful parameters for a porous membrane, which can be used as a filter in the treatment of waste-water, water purification, etc., [6]. So, knowledge of this

parameter, allows us to choose an appropriate membrane with reference to the size of the particles to be separated. The pore perimeter based on pore diameter is then calculated and given below:

$$l_p(\mu) = \pi, D_{eff} \tag{5}$$

As we have calculated the porosity of the graphite foam directly from the binary image in section 2.3, the mathematical expression for the calculation of the porosity in the IAM can be defined here as the ratio of the number of white pixels (i.e., pore regions) to the number of pixels in the entire image as follows:

$$\emptyset = \frac{n_w}{LW} \tag{6}$$

where $\emptyset$, the porosity, n_W is the number of white pixels, while *L* and *W* are the length and width of the image, respectively.

In this section we have calculated the effective thermal conductivity (ETC) of graphite foam. This is one of the most important thermal properties of porous materials that is based on the equations derived from the basic heat transfer equations. The effective thermal conductivity k_{eff} can be calculated by using the equations proposed in [25,26], i.e.,

$$\mathrm{k}_{eff} = k_{wall}\, \rho_{\mathrm{r}}\, \bar{f}z \quad \text{(W/m.K)} \tag{7}$$

Where k_{wall} is the cell wall thermal conductivity, and ρ_{r} and $\bar{f}z$ are the relative density and shape factor of the porous material, respectively.

In order to simulate the ETC of metallic foams, three-dimensional polyhedral geometries for porous materials, in which the ETC lies between the effective medium theory model [25] and the Hashin-Shtrikman upper bound [26], are used as follow:

$$K_{eff}^{low} = \begin{cases} 0, & 0 < \rho_{\mathrm{r}} < 1/3 \\ \frac{3\rho_{\mathrm{r}}-1}{2} K_{wall}, & \frac{1}{3} < \rho_{\mathrm{r}} < 1 \end{cases} \quad \text{Effective Medium Theory}$$

$$K_{eff}^{up} = \frac{2\rho_r K_{wall}}{3-\rho_r} \qquad \text{Hashin – Shtrikman upper bound} \tag{8}$$

The relative density ρ_{r} is defined as the ratio of the volume of the cell wall to the total volume i.e.,

$$\rho_{\mathrm{r}} = \frac{V_{solid}}{V_{total}} \tag{9}$$

By substituting Eq. (8) into Eq. (7), the theoretical bounds for the shape factor $\bar{f}z$ are given by:

$$\bar{f}z^{low} = \begin{cases} 0, & 0 < \rho_{\mathrm{r}} < 1/3 \\ \frac{3\rho_{\mathrm{r}}-1}{2\rho_{\mathrm{r}}}, & \frac{1}{3} < \rho_{\mathrm{r}} < 1 \end{cases} \text{, Effective Medium Theory} \tag{10}$$

$\bar{f}z^{up} = \frac{2}{3-\rho_r}$, Hashin – Shtrikman upper bound (11)

Finally, by substituting the values obtained by IAM and using other physical properties of graphite foam in the above relations, the physical properties and the thermal conductivity of the sample are obtained.

2.5. Virtual 3D Reconstruction

2.5.1. Virtual 3D model construction of the sample

In this section we described the use of a 3D reconstruction method using X-ray micro-computed tomography (μCT), slice images, and Imorph open source software so as to analyze the graphite foam microstructure. The value of the porosity and SSA of graphite foam were obtained using this 3D model. The virtual 3D reconstruction of graphite foam is useful so that we can achieve a deep understanding of graphite foam microstructure and physical properties such as porosity, SSA, pore size, tortuosity and so on. It readily provides cross sections of its struts and their areas and gives information about a strut's shape and size. In this way we have prepared the sample for imaging operations and obtained 1287 2D cross sectional slice images of graphite foam.

The images taken by this method include noises. These noises may increase after the image binarization process, and this can be reduced using image filtering techniques. Such noise reduction is a typical pre-processing step that improves the accuracy of the results. After removing such noises, the region of interest (ROI) on the slice images is determined and then the proper thresholding value on the imported slice images, based on the changing of the histogram on the pore and solid region, is adjusted. It should be noted that choosing the proper ROI is of great importance. As we used a lot of slice images (1287 slices) for a 3D model reconstruction, then the bigger ROI means there will be lots of voxels included in the 3D model, so this will require a robust processor for its analysis. On the other hand, by choosing the proper ROI we have separated unnecessary areas like the scale bar and the border of the images (which shouldn't be included in the image analysis stages). To make a visible 3D model, the pore and solid phases are meshed onto the stack images. The virtual 3D reconstructed model of graphite foam and its reconstruction procedure are shown in Figs. 9 and 10, respectively.

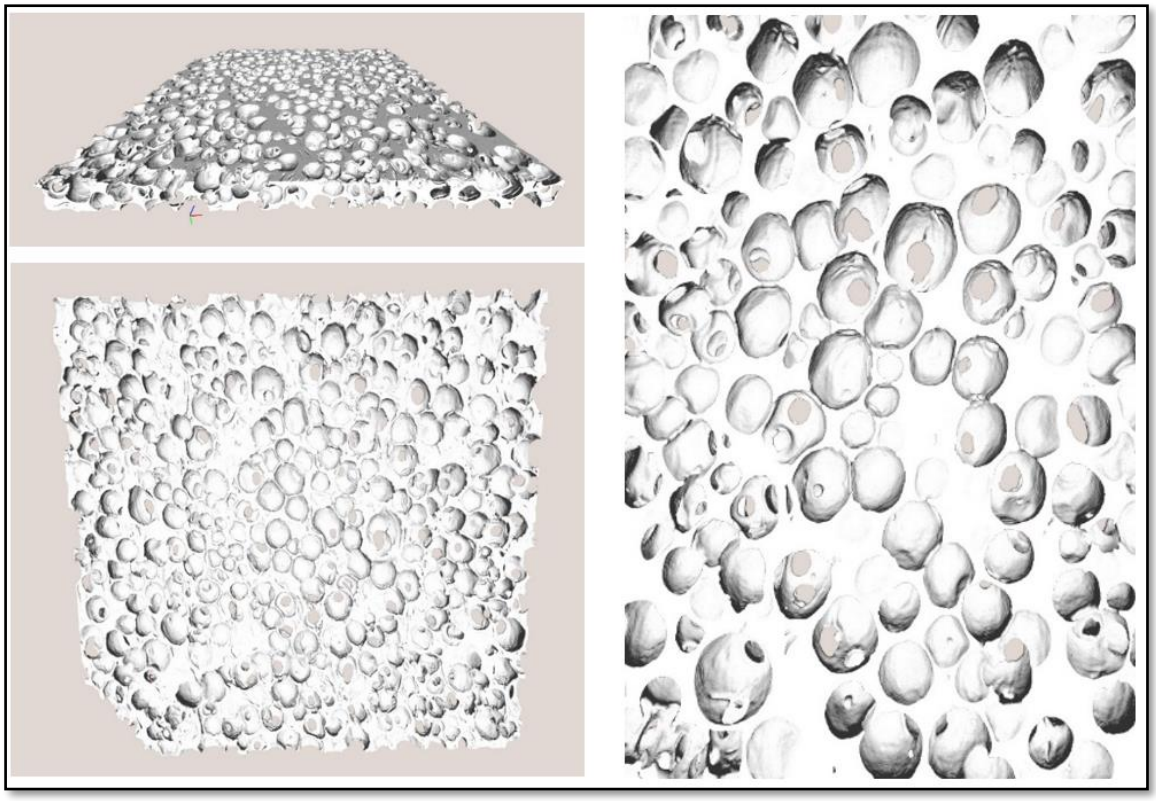

Fig. 9 The virtual 3D reconstructed model of graphite foam in different views

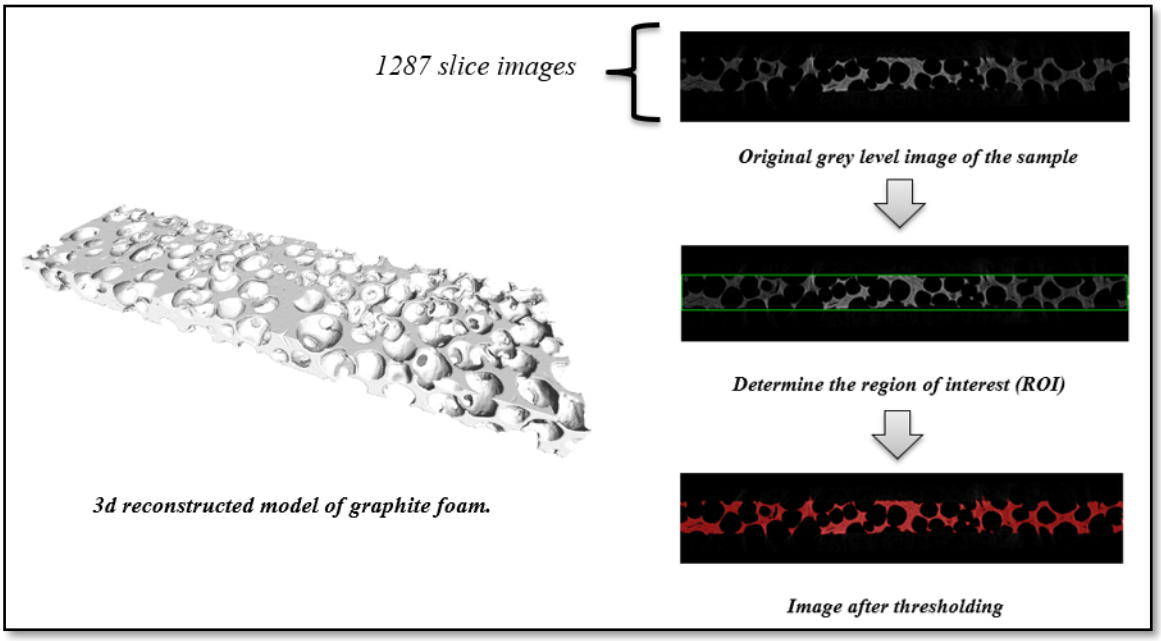

Fig. 10 The procedure of virtual 3D reconstruction of graphite foam

2.5.2. Extracting the geometrical & physical properties

Since we made a virtual 3D reconstructed model of our graphite foam sample, we will be able to calculate its physical properties from the simplest to the most sophisticated ones directly using the Imorph software. These morphological parameters are the porosity, the SSA, the strut cross section, the tortuosity, the sample skeleton, etc. For computing the total porosity, the number of voxels in each phase (Pore and Solid phases) of the 3D model are counted. Then the porosity is calculated based on the fraction of pore and solid phases. It should be noted that the reconstructed model consists of the sum of the voxels in both pore and solid phases. In section 2.5.1., while we have meshed the surface of pore and solid phases of the model by a reconstruction procedure, we obtained similarly the value of SSA as an output. We're also be able to calculate the effective thermal conductivity of graphite foam once again by using the measured data in this section (e.g., the values of porosity and the average pore diameter) as input in the equations derived from the fundamental heat transfer equations described in section 2.4.

2.6. Laboratory Methods

There are also many traditional experimental methods for characterizing the pore morphology and calculation of its basic geometrical and physical parameters. These methods include the microscopic method, mercury porosimetry, Archimedean porosimetry, and the Brunauer-Emmett-Teller (BET) method. In this section we used the BET method, as opposed to the IAM method, on prepared samples of graphite foam at DAYTAM research center, Ataturk university. The aim of the BET theory is to explain the physical adsorption of gas molecules on a solid surface. It serves as the basis for an important technique for analyzing the measurement of the BET surface area and other pore parameters of materials. The BET theory applies to systems of multilayer adsorption and usually utilizes probing gases that do not react chemically with material surfaces as adsorbates to quantify specific surface area. Nitrogen is the most employed gaseous adsorbate used for surface probing by BET methods. The BET method is widely used in surface science for the calculation of surface areas of solids by physical adsorption of gas molecules. Observe that the ISO 9277 standard for calculating the specific surface area of solids is based on the BET method. The device used in this method and the process of gas adsorption and desorption are shown in Fig. 11. In this work, we also obtained the average pore diameter, the cumulative pore volume, and the BET surface area, all using the BET method.

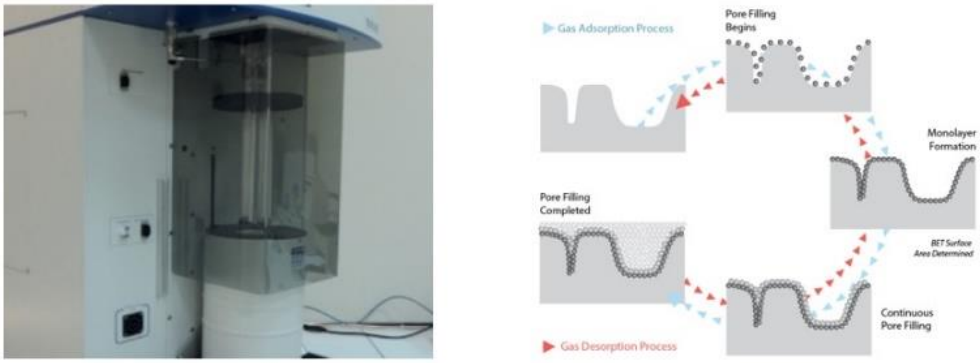

Fig. 11 The BET surface area measurement machine and the gas adsorption, desorption process (Particle technology labs)

3. Results and Discussion

At the outset we implemented the image analysis method on 2D SEM images. It was observed that the results are not precise using SEM images of graphite foam composed of macro pores. As shown in Fig.12, on the binarized image (right), except for a few areas of pores (marked in red), most of the pores are not identified and distinguished from non-pore areas using IAM on SEM images. Since the graphite foam sample we studied is composed mostly of macro pores and that the minimum magnification on SEM is very high, then the provided images included a limited number of pores with a large cell area compared to the CT images that include a large number of pores in a single image with more distinguishable pore and non-pore regions. This factor allows for the possibility to count all the existing pores in the entire surface of the sample. The information about the distribution of the morphological parameters such as pore size, the perimeter and the area are then provided statistically in a precise manner. In addition, the prepared SEM images are also influenced by the electron beam in the imaging procedure which, in itself, creates more noises and white areas beside the pore regions. In fact, this can make the pores appear to be connected to each other in the images. Consequently, considering the statistical analysis and pixel counting operations (in pore and non-pore regions), the accuracy of the determination of the local maximum value (M, at the center of each pore blob) and the calculation of the porosity are affected greatly and that then causes some errors.

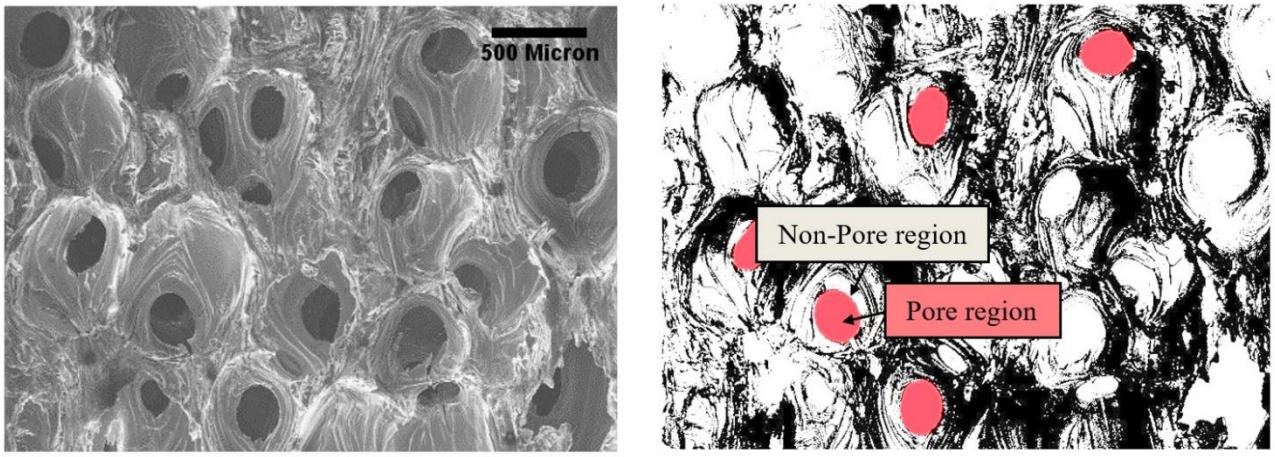

Fig. 12 The original SEM and binarized image of graphite foam sample

Given that the results obtained using SEM images are not more accurate, the proposed IAM is implemented on the images taken by *X-ray μCT*, as shown in Fig.5. The results indicate that unlike SEM images, there are a lot of pores in a single image which are, in fact, distinguishable. The amount of noise is reduced by applying a filter. After that, parameters like local maximum value (***M***) for each pore blob is computed as an input value for the calculation of physical properties including; the effective pore diameter (D_{eff}**)**, the area of a pore blob (A_P**)**, the perimeter of pores (l_P**)**, the porosity (∅), and effective thermal conductivity (ETC). The computed pore parameters, ETC and SSA of graphite foam and their distributions (from the 3D model) are shown in Table 2 and Fig. 13, respectively.

Table 2. The computed pore parameters, the physical properties and thermal conductivity of graphite foam obtained with IAM.

Graphite Foam	D_{eff} µm	A_P mm²	$l_P(\mu m)$	SSA S_V (m^2/m^3)	ETC K_{eff} (W/m.K)
Mean	527.76	0.23	1658.023	4734.62	43.41
Minimum	210.73	0.03	662.043		
Maximum	873.04	0.59	2742.751		

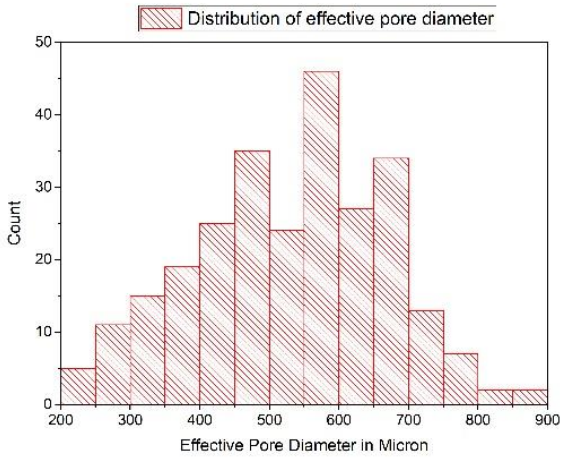

(a)

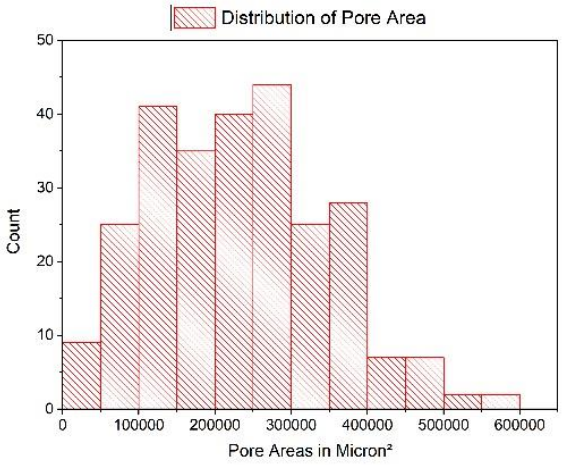

(b)

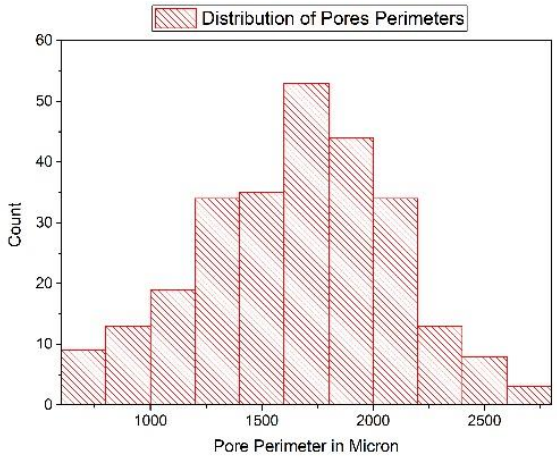

(c)

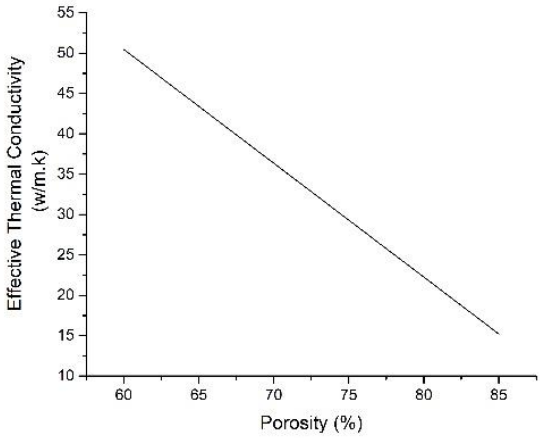

(d)

Fig. 13 The distributions of the parameters of pore morphologies; (a) the effective pore diameter, (b) the area, (c) the perimeter and (d) the Porosity-Effective thermal conductivity relationship

The variation of the effective thermal conductivity of graphite foam with porosity ranging from 60% to 85% is shown in Fig. 13(d). For different values of the porosity, Eq.7 is employed to compute the thermal conductivity. The total porosity values of the graphite foam we studied and obtained from three different methods are given in Table. 3 and compared with the data supplied by the manufacturer. The results indicate that IAM and virtual 3D reconstructed methods are suitable to characterize the total porosity. As is expected, the 3D model provides the most efficient approach to achieve accurate results that are very close to the data supplied by the manufacturer. Note that the main reason we focused on comparing different porosity values using different methods is because many physical and thermal properties strongly depend on the porosity.

Table 3. The comparison table of total porosity values obtained from the 2D SEM and μCT images, the 3D model, and the Manufacturer

Total porosity Ø (%)			
Manufacturer POCO	2D IAM (μCT images)	3D Model	2D IAM (SEM images)
75.0	68.90	71.22	85-90

3. Conclusion

In this work, both the advanced image analysis technique and the virtual 3D reconstruction method are employed for the calculation of the physical properties and the thermal conductivity of graphite foam. The laboratory method used BET in order to determine the average pore size, cumulative pore volume, the BET surface area, etc. It is found that, theoretically, there is a direct relationship between the porosity and the thermal conductivity of graphite foam.

The results drawn from the IAM, the Virtual 3D reconstructed model, and the manufacturer data are compared. It is found that the IAM is an inexpensive, nondestructive, and accurate method for the study of graphite foam material compared to other experimental methods. In addition, it is found that experimental methods do not generally lead to satisfactory results as far as closed-cell porous material is considered. Geometrical parameters and information about each individual pore cannot be determined experimentally.

On the other hand, we can use a reconstructed virtual 3D model of porous materials on commercial software for studying heat transfer, fluid flow, and mechanical strength analysis. The proposed methods can be implemented so as to predict the physical properties and the thermal conductivity of porous materials. As a result, theoretical studies about the porous materials used in various industries can be conducted robustly and inexpensively.

Nomenclature

k_{wall}	Cell Wall Thermal Conductivity
D_{eff}	Effective Pore Diameter
k_{eff}	Effective Thermal Conductivity
LW	Length and Width of the Image
n_w	Number of White Pixels
l_P	Pore Perimeter
A_P	Pore Area
$\bar{f}z$	Shape Factor

Greek Letters

$\emptyset$	Porosity
ρ_r	Relative Density

Acknowledgements

This research is supported by the Scientific and Technological Research Council of Turkey under the grant number 315M136.

References

[1] P.S Liu, G.F Chen, Porous Materials, 1st edn. (Elsevier, 2014), pp. 1-20. https://doi.org/10.1016/B978-0-12-407788-1.00001-0

[2] W. Lin, J. Yuan, B. Sundén, (Linköpings universitet, Sweden, 2011), pp. 748-755. https://doi.org/10.3384/ecp11057748

[3] Y. Zhong, Q. Guo, S. Li, J. Shi, L. Liu, Sol Energ Mat Sol C. 94: 1011 (2010)

[4] J. Kim, E. Jeong, Y. Lee, J Ind Eng Chem. 32, 21 (2015)

[5] J. Banhart, Prog. Mater. Sci. 46: 559 (2001), https://doi.org/10.1016/S0079-6425(00)00002-5

[6] F.H. She, K.L. Tung, L.X. Kong, Robot CIM-INT Manuf. 24: 427 (2008)

[7] P. Elia, E. Nativ-Roth, Y. Zeiri, Z.'e. Porat, Microporous Mesoporous Mater, 225: 465 (2016)

[8] Borislav D. Zdravkov, Jirı J. Cermak, Martin Sefara, Josef Janku, Cent. Eur. J. Chem., 5: 385 (2007), https://doi.org/10.2478/s11532-007-0017-9

[9] K. Sakai, J Membrane Sci, 96: 91 (1994)

[10] R. Ziel, A. Hausa, A. Tulkeb, J Membrane Sci, 323: 241 (2008)

[11] Z. Ying, M. Jürgen, Ceram. Int., 42: 2861 (2016), https://doi.org/10.1016/j.ceramint.2015.11.015

[12] P.S. Liu, Philos. Mag, 90: 447 (2010), https://doi.org/10.1080/09500831003745571

[13] K.S. Walton, R.Q. Snurr, J. Am. Chem Soc, 129: 8552 (2007)

[14] Herbert Giesche, Part Part Syst Char, 23: 9 (2006)

[15] Marcelo de Assumpção Pereira-da-Silva, Fabio A. Ferri, Nanocharacterization Techniques, (Elsevier, 2017), pp. 1-35. https://doi.org/10.1016/B978-0-323-49778-7.00001-1

[16] X. Zhu, S. Ai, D. Fang, B. Liu, X. Lu, Comput. Mater. Sci, 82: 451 (2014)

[17] J. Wawrzeńczyka, W. Kozak, Procedia Eng, 108: 102 (2015)

[18] W. D. Martin III, B. J. Putman, N. B. Kaye, Constr Build Mater, 48: 210 (2013)

[19] C. Perrot, R. Panneton, X. Olny, J. Appl. Phys, 101: 113538 (2007)

[20] P. De Jaeger, C. T'Joen, H. Huisseune, B. Ameel, M. De Paepe, J. Appl. Phys, 109: 103519 (2011)

[21] Karthik. K. Bodla, Suresh. V. Garimella, Jayathi. Y. Murthy, Int. J. Heat Mass Transf, 73: 250 (2014)

[22] M. Bracconi, M. Ambrosetti, M. Maestri, G. Groppi, E. Tronconi, Chem. Eng. Trans, 315: 608 (2017)

[23] X. Zhu, S. Ai, X. Lu, K. Cheng, X. Ling, L. Zhu, B. Liu, Comput. Mater. Sci., 85: 38 (2014)

[24] E. Baird, G. Taylor, Curr. Biol, 27: 289 (2017)

[25] M. Ma, H. Ye, Appl. Therm. Eng. 73: 1277 (2014)

[26] P. Kumar, F. Topin, J. Vicente, Int J Therm Sci., 81: 13 (2014)

[27] James. K. Carson, Simon. J. Lovatt, David. J. Tanner, Andrew. C. Cleland, Int. J. Heat Mass Transf., 48: 2150 (2005)

[28] Z. Hashin, S. Shtrikman, J. Appl. Phys, 33: 3125 (1962)

[29] X. Yang, T. Lu, T. Kim, Transport Porous Med., 100: 211 (2013)

[30] R. Lind, Open Source Software in Life Science Research, (Elsevier, 2012), pp. 131-149. https://doi.org/10.1533/9781908818249.131

[31] E. Brun, J. Vicente, F. Topin, R. Occelli, iMorph: A 3D Morphological Tool to Fully Analyze All Kind of Cellular Materials (in Cellmet'08, Dresden, Germany, 2008)